energies

MDPI

Article

Acceleration of Biohydrogen Production During Dark Fermentation Using Microbial Immobilised Biochar–Alginate Beads

Jessica Quintana-Najera [1,2], Jaime E. Borbolla-Gaxiola [2,*] and Andrew B. Ross [1,*]

[1] School of Chemical and Process Engineering, University of Leeds, Leeds LS2 9JT, UK; j.quintana@uas.edu.mx
[2] Faculty of Chemical and Biological Sciences, Autonomous University of Sinaloa, Culiacan 80100, Mexico
* Correspondence: j.borbolla@uas.edu.mx (J.E.B.-G.); a.b.ross@leeds.ac.uk (A.B.R.)

Abstract

The transition to renewable energy requires scalable and sustainable hydrogen production technologies. Dark fermentation (DF) can generate biohydrogen from diverse biomass feedstock, but its efficiency remains limited. Immobilising anaerobic consortia offers a route to improve performance. This study reports on the immobilisation of whole cells in hybrid biochar–alginate beads (BAB) compared with control alginate beads (CAB) during DF. Biochar from oakwood and water hyacinth, pyrolysed at 450 and 600/650 °C, were incorporated into BAB. BAB increased biohydrogen production rates by 1.4–2.6-fold relative to CAB, driven by enhanced microbial attachment, synergistic interactions, and improved mass transfer. High-temperature biochar generated the strongest effects, raising hydrogen yield by up to 23% and shortening the lag phase by 94%. Biochar properties, including porosity, surface area, inorganic content, electrical conductivity and buffering capacity, likely support these effects. These results establish hybrid biochar-alginate support as a promising platform to accelerate DF and advance biohydrogen as a sustainable biofuel.

Keywords: biohydrogen; biochar–alginate beads; dark fermentation; cell immobilisation

1. Introduction

The accelerating accumulation of greenhouse gases (GHG) and the resultant global warming and climate crisis underscore the necessity of a paradigm shift from fossil fuel dependence towards scalable renewable energy alternatives. Hydrogen (H_2) has emerged as a cornerstone of the sustainable energy sector due to its high gravimetric energy density (142 MJ/kg) and zero-emission profile at the point of use. Its storability, reactivity, and compatibility with existing infrastructures make it an attractive energy carrier for power, heat, and transport. However, its production currently relies heavily on natural gas and coal, resulting in substantial CO_2 emissions. The contribution of H_2 towards a sustainable future can be broadly divided into two categories: i) production from renewable energy and biogenic pathways, and ii) deployment for heat, power and transport. Sustainable biohydrogen production from biomass and other low-cost sources has therefore become a major research priority [1].

Biomass-derived biohydrogen can be obtained through thermochemical (e.g., gasification, pyrolysis, aqueous-phase reforming), electrochemical (electrolysis), and biological routes (biophotolysis, photo-fermentation, or dark fermentation [DF]). Thermochemical processes typically generate syngas (CO, CO_2, H_2, CH_4), whereas biological pathways

Academic Editor: Marcin Dębowski

Received: 23 April 2026
Revised: 18 June 2026
Accepted: 19 June 2026
Published: 23 June 2026

yield biohydrogen along with organic acids, alcohols, and biogas [2]. Biophotolysis utilises the [Fe-Fe]-hydrogenase enzymes of photosynthetic organisms, such as plants, cyanobacteria, and algae, to split water, while photo-fermentation exploits nitrogenase activity in light-driven bacteria to reduce molecular hydrogen and protons into H_2 [3]. Conversely, DF operates under anaerobic conditions without external light, relying on hydrogenase enzymes ([Ni-Fe] and [Fe-Fe]) to oxidise energetic molecules, such as carbohydrates, into H_2 and by-products such as volatile fatty acids (VFAs) and alcohols [4]. While thermochemical and electrochemical routes are well-established, sustainable DF is increasingly attractive due to its low cost, mild operating conditions, short retention times, and capacity to harness diverse feedstocks ranging from lignocellulosic residues to municipal and agricultural wastes [5].

However, these technologies face distinct techno-economic barriers that must be overcome to achieve economic competitiveness and operational feasibility. Thermochemical routes such as pyrolysis and gasification are often hindered by tar formation and organic impurities in the syngas, which introduce severe operational challenges. Gasification is also characterised by high capital investment, equipment corrosion, and catalyst deactivation. Meanwhile, water electrolysis remains highly electricity-intensive, which severely limits its economic viability. The development of photobioreactors and the optimisation of biophotolysis also encounter economic and technological hurdles due to the capital-intensive nature of the processes and the difficulties associated with scaling up. Regarding DF, the pretreatment of the inoculum can be costly, and the technology still requires significant process development to design functional bioreactors capable of overcoming thermodynamic limitations. Consequently, various strategies have been proposed to improve fermentative H_2 production, including genetic engineering for obtaining highly productive bacterial strains, cell immobilisation, and process integration to enhance overall economic viability [6].

The performance of DF is fundamentally shaped by substrate composition, inoculum origin, and operational conditions [7]. Mixed microbial consortia, commonly derived from sewage sludge or manure, provide synergistic metabolic activity but also harbour hydrogen-consuming methanogens, which must first be inactivated via heat shock, aeration, microwave or ultrasonic treatment. Following this pretreatment, the most efficient H_2 producers proliferate, predominantly sporulating obligate anaerobes from the genus *Clostridium*, which employ acetate and butyrate fermentative pathways [2]. Among the various reactor configurations utilised for DF, continuous stirred-tank reactors (CSTR) operating with suspended cells are among the most common. However, CSTRs are heavily constrained by cell washout at short hydraulic retention times (HRTs). Cell immobilisation offers a robust solution to these issues by maintaining high biomass densities, improving process stability, and enabling more compact reactor designs [8]. Numerous supports and matrix configurations have been proposed to incorporate functional materials for immobilisation in DF, including alginate-chitosan-SiO_2 composites in CSTR [9], carbon nanotubes (CNTs) and activated carbon (AC) in an up-flow anaerobic sludge blanket (UASB) bioreactor [10], alginate and chitosan magnetite-functionalised nanoparticles [11], polyester fibre particles [12], as well as expanded clay, ceramics and, charcoal [13–15].

Immobilisation enhances process resilience by protecting the microorganisms from shear stress, promoting biofilm formation, mitigating cell washout, and facilitating mass transfer [16]. Common strategies include entrapment within semipermeable polymer matrices such as alginate—a biocompatible polysaccharide produced by algae and bacteria (*Pseudomonas* and *Azotobacter*) that is composed of alternating D-mannuronic and L-guluronic acid residues [17]. While this remains a prevalent method due to its mild gelation conditions, conventional alginate beads face significant industrial challenges, including mechanical fragility, mass-transfer resistance and inability to stimulate enzymatic activity.

Alternatively, immobilisation on functional porous carriers via adsorption enables rapid microbial colonisation while permitting unhindered nutrient exchange [18]. Ideal carrier properties include material functionality, superior biomass-loading capacity, long-term durability, and minimal mass transfer resistance [12].

Biochar (BC), a low-cost carbonaceous material produced through the oxygen-limited pyrolysis of biomass, offers an elegant solution to these limitations and has emerged as a promising additive and immobilisation support in anaerobic systems [19,20]. Its physicochemical properties—determined by the choice of feedstock and specific pyrolysis conditions—include high porosity, a large surface area (SA), diverse functional groups, high electrical conductivity, and an inherent buffering capacity [16]. Pyrolysis temperature is crucial in determining the SA and porosity of biochar, which are among its most critical features for exploring applications. The SA dictates the cation exchange capacity (CEC) and overall reactivity of the biochar, as a higher SA facilitates access to surface charges and reactive sites, while the porosity governs its water-holding capacity [21]. Furthermore, the thermal decomposition of biomass is accompanied by the loss of oxygen- and hydrogen-containing functional groups and the subsequent formation of aromatic structures, a process that intensifies with increasing process severity [22]. These structural properties confer redox activity, thereby facilitating direct interspecies electron transfer (DIET) via oxygenated functional groups (OFGs) such as quinone–hydroquinone moieties [23].

Although biochar can be derived from a wide variety of biomass materials, this study focuses on two distinct feedstocks—oak wood (OW) and water hyacinth (WH)—to explore how biomass architecture and pyrolysis temperature interact to influence DF performance. Given the lignocellulosic nature of oak wood, its resulting biochar possesses excellent mechanical rigidity and a well-defined microporous framework, serving as a robust scaffold for microbial colonisation. Conversely, water hyacinth, in addition to its lignocellulosic constituents, is predominantly composed of starch, sugars, pectin, proteins and lipids. Native to tropical America, WH is one of the most invasive and damaging aquatic macrophytes worldwide, having spread across nearly 100 countries; it is notoriously difficult to eradicate due to its rapid growth rate and adaptability to extreme environments. Under nutrient-rich conditions, WH can double its biomass within two weeks, reaching growth rates of 50–72 g DW/m^2·day (equivalent to 18–26 kg/m^2·annum). This rapid proliferation underscores the urgent necessity for its valorisation as a sustainable biomass source with industrial applications aligned with circular economy frameworks [24]. Consequently, converting WH into biochar—a functional and versatile material applicable to environmental bioremediation, agriculture, biomaterials, and biofuel generation—presents a highly attractive avenue of research [25]. While biochar can effectively adsorb and host microbial populations, adsorption alone is often slow and offers limited control over biomass loading. Entrapment within polymer matrices can overcome these limitations; thus, integrating adsorption (via biochar) with entrapment (via alginate) has the potential to stabilise microbial communities, maintain strictly anaerobic microenvironments, and significantly enhance biohydrogen productivity [18].

Even though alginate encapsulation and biochar amendment have individually been reported to improve biohydrogen yields in DF, their integration into a hybrid immobilisation platform remains largely unexplored. To the best of our knowledge, this study is the first to combine oak wood and water hyacinth biochars with alginate to produce composite beads specifically engineered for microbial immobilisation in successive runs of DF. Herein, this work evaluates the feasibility of these biochar–alginate beads as a robust immobilisation system for DF, utilising biochars produced at both intermediate (450 °C) and high (600/650 °C) pyrolysis temperatures. This approach allows the identification of specific structural and chemical properties governed by pyrolysis conditions that underpin

enhanced biohydrogen production. Ultimately, this hybrid adsorption–entrapment strategy offers a novel pathway to overcome long-standing thermodynamic and operational limitations in DF, thereby advancing microbial immobilisation technologies and accelerating sustainable biohydrogen production.

2. Materials and Methods

2.1. Source and Pre-Treatment of Inoculum

Anaerobic sludge was collected from the mesophilic wastewater treatment plant at Esholt (Bradford, UK). To suppress methanogenic activity, the sludge was autoclaved at 115 °C for 30 min (CertoClav, Leonding, Austria, A-4050) and subsequently stored at 37 °C until use. The effectiveness of this thermal pretreatment was verified using sodium acetate as a substrate. Biohydrogen production pathways typically involve the conversion of pyruvate into acetic and butyric acid, whereas the selected microbial consortia lack the capacity to metabolise acetate directly. Conversely, methanogens possess the capability to convert acetate into methane via acetoclastic methanogenesis [26]. Fermentation of the heat-treated sludge with sodium acetate resulted in negligible biohydrogen yields (~3 mL H_2/g VS), confirming the successful inactivation of methanogens. Prior to the DF experiments, the sludge was centrifuged at 4000 rpm for 5 min, resuspended in an equal volume of distilled water, and sieved through a 1 mm mesh. The volatile solids (VS) concentration of the inoculum was 29.69 g VS/L, as determined gravimetrically [27].

2.2. Biochar Production

Water hyacinth (*Pontederia crassipes*) was harvested from Lake Victoria, Uganda, and supplied by The Centre for Research in Energy and Energy Conservation (CREEC). Biochar was produced via slow pyrolysis at 450 °C and 600 °C for 1 h, yielding WH-BC450 and WH-BC600, respectively. Bark-free holm oakwood residue was obtained from a commercial supplier (Proininso, Malaga, Spain) and pyrolysed in a mono-retort kiln at 450 and 650 °C, generating OW-BC450 and OW-BC650. To ensure experimental homogeneity, all biochar samples were ground and sieved to particle sizes <500 µm.

2.3. Biochar Characterisation

The biochars used in this experiment were characterised as described previously [28] as exhibited in Table 1. The proximate composition was determined using a thermogravimetric analyser (TGA/DSC 1, Mettler Toledo, Tokyo, Japan). Elemental analysis (CHNS) was performed with an automatic Thermo Instruments Flash EA 1112 Series analyser (Thermo Scientific, Waltham, MA, USA); results are expressed as a percentage of total dry weight, with total oxygen (O) determined by difference. Surface area (SA) was measured by gas adsorption using a Tristar 3000 CI2 (Micromeritics, Norcross, GA, USA) at 273 K, applying non-local density functional theory (NLDFT) models for infinite slit carbonaceous materials [29]. Surface functionality was determined in ultra-high vacuum (10^{-9} Pa) using an X-ray photoelectron spectroscopy (XPS) Specs system with a high-intensity XR50 X-ray monochromatic Al Kα (1486.71 eV) source and a Phoibos 150 hemispherical electron analyser (SPECS Surface Nano Analysis GmbH, Berlin, Germany). Survey spectra were acquired with a pass energy of 25 eV (0.1 eV steps; 0.1 s dwell time). High-resolution C 1 s, O 1 s and N 1 s spectra were obtained with a pass energy of 3 eV. CASA XPS software (Casa Software Ltd., Devon, Japan, version 2.3.17) and Tougaard Background subtraction were utilised for curve fitting.

Inorganic analysis was conducted via X-ray fluorescence (XRF). Sample preparation started with homogenisation by calcination of the biochars in a muffle furnace (Nabertherm B80, Nabertherm GmbH, Lilienthal, Germany) at 550 °C for 2 h, followed by 850 °C for

2 h. The resulting ashes were ground with a mortar and pestle and stored in a desiccator. For the analysis, 0.7 g of ash sample was mixed with 6.3 of lithium borate flux into a platinum crucible, heated to 1100 °C, and fused into beads using a Katanax K1 automated fusion system (Katanax Inc., Québec City, QC, Canada). The beads were then analysed by wavelength-dispersive X-ray fluorescence (WDXRF) on a Rigaku Primus WDXRF 1 system (Rigaku, Akishima-shi, Japan). Inorganic element concentrations are expressed in mg/kg (ppm) as detailed in Table 2.

Table 1. Chemical, physical and functional composition of the biochars expressed in dry basis. Values obtained from Quintana-Najera [28].

Chemical and Physical Composition										
Biochar	pH	VM (%)	FC (%)	Ash (%)	C (%)	H (%)	N (%)	O (%)	S (%)	SA (m^2/g)
OW-BC450	9.9	21.1	67.2	11.7	65.7	2.7	0.6	19.3	0.0	221
OW-BC650	9.3	11.8	73.9	14.3	76.5	1.4	0.8	7.0	0.0	237
WH-BC450	9.1	30.9	35.2	33.9	26.1	1.4	1.7	36.9	0.2	39
WH-BC600	10.6	21.5	35.9	42.6	37.8	1.0	2.0	14.9	0.0	99
XPS surface functionality analysis										
		Survey			C 1 s					
Biochar		C 1 s (%)	O 1 s (%)	N 1 s (%)	C-C (%)	C-O (%)	C=O (%)	COO (%)	π-π*	
OW-BC450		81.1	16.0	1.2	23.5	22.1	35.9	2.6	15.9	
OW-BC650		78.6	17.0	0.9	24.1	38.8	37.1	-		
WH-BC450		58.0	21.2	3.3	22.5	49.9	16.4	16.4		
WH-BC600		67.3	18.9	1.5	45.0	31.5	8.8	7.8		

VM—volatile matter, FC—fixed carbon, SA—surface area. Survey XPS spectra: C 1 s (284 eV), O 1 s (532 eV) and N 1 s (399 eV); C 1 s XPS spectra: aromatic C-C (284.4–285.2 eV), C-O (286.1–286.6 eV), C=O (287.6–288.2 eV), COO (288.8–289.3 eV), and π-π* (291.3 eV) [30].

Table 2. Inorganic element analysis of biochars determined by X-ray fluorescence.

Biochar	Inorganic Elements (mg/kg)																		
	Fe	K	Ca	Mg	Al	Si	P	S	Na	Ni	Cl	Mn	Co	Cu	Sr	Mo	Ba	Ti	Zn
OW450	29,105	3896	30,470	2912	265	637	936	361	358	2429	0	890	66	117	108	94	0	0	11
OW650	3305	5141	71,823	5168	1274	4016	2757	598	809	268	83	898	0	38	329	19	0	129	22
WH450	20,403	10,393	8633	1276	25,996	53,803	1035	978	1083	232	934	755	0	32	64	0	659	1556	30
WH600	40,826	23,633	41,267	4924	30,563	52,234	3102	2426	2216	968	10,698	1893	41	77	278	64	0	0	89

2.4. Immobilisation

Alginate beads were prepared by extruding alginate–cell suspensions into a cross-linking bath to induce gelling. Biochar–alginate beads (BAB) and control alginate beads (CAB) were produced following Smidsrød and Skjåk-Bræk [31], with minor modifications. Briefly, 30 mL of 2% (*w*/*v*) sodium alginate—containing 2% (*w*/*v*) of either oak wood or water hyacinth biochar (BAB) or no biochar (CAB)—was mixed with 30 mL of inoculum suspension under continuous stirring, yielding a final volume of 60 mL. The mixture was extruded through a pipette (0.8–0.9 mm tip diameter) into a 0.1 M $CaCl_2$ solution. The resulting gel beads (3–6 mm diameter) were allowed to harden for 30 min. The final bead composition comprised 20 g VS/L, alginate 1%, and biochar 1% (*w*/*v*). Beads were thoroughly washed, resuspended in distilled water, and incubated at 37 °C until required.

2.5. Reactor Setup

Biohydrogen production was monitored using an Automatic Methane Potential Test System (AMPTS II; Bioprocess Control, Lund, Sweden). Each reactor was loaded with a 1:3 ratio of beads to distilled water (60 mL of drained BAB or CAB and 180 mL of distilled water), resulting in a final inoculum concentration of 5 g VS/L and a biochar dosage of 0.25% (*w*/*v*). Glucose was supplied at 5 g VS/L, providing an inoculum-to-substrate ratio (ISR) of 1. The initial pH was adjusted to 6.0 using phosphoric acid (>85% purity) where necessary. Reactors were maintained at 37 °C in a thermostated water bath, purged with nitrogen to ensure anaerobic conditions, and stirred automatically for 60 s every 10 min. Produced CO_2 was removed via absorption in a 3 M NaOH trap, while H_2 was measured volumetrically and normalised to standard conditions (273 K, 1 atm) by the AMPTS software (version AMPTS II light software). Negative controls (sludge immobilised in CAB without substrate) were included to account for H_2 from residual substrate or alginate utilisation; however, production was negligible. Positive controls (substrate-fed CAB) were used to isolate the effect of biochar amendment. All treatments were performed in triplicate (Table 3). At the end of each batch, reactors were opened, the supernatant was collected for analysis, and the beads were replenished with distilled water and fresh substrate for a second cycle, replicating the same fermentation conditions. The OW-BC450 system was excluded from the second run due to its similarity with the OW-BC650 system in the first batch and limitations in reactor availability.

Table 3. Description of experimental conditions.

System	Description	Biochar	Substrate
OW450	Biochar–alginate bead	OW-BC450	√
OW650	Biochar–alginate bead	OW-BC650	√
WH450	Biochar–alginate bead	WH-BC450	√
WH600	Biochar–alginate bead	WH-BC600	√
CAB	Control alginate bead	X	√
Blank	Blank alginate bead	X	X

2.6. Kinetic Analysis

The cumulative biohydrogen yield, determined according to Equation (1), was fitted to the modified Gompertz model (Equation (2)) to characterise the hydrogen evolution kinetics [32]. Within this model, H(t) represents the cumulative biohydrogen yield (mL H_2/g VS) at a given time t (h). The kinetics parameters derived from the model include H_{max}, maximum biohydrogen potential (mL H_2/g VS); R_{max}, the maximum specific biohydrogen production rate (mL H_2/g VS·day); and λ, duration of the lag phase (h).

$$H_2 = \frac{\text{Volume } H_2 \text{ from sample (mL)} - \text{Volume } H_2 \text{ from blank (mL)}}{\text{Substrate VS Concentration } \left(\frac{g}{L}\right) \times \text{Working volume (L)}} \quad (1)$$

$$H(t) = H_{max} \cdot \exp\left\{-\exp\left[\frac{R_{max} \cdot \exp(1)}{H_{max}}(\lambda - t) + 1\right]\right\} \quad (2)$$

2.7. Volatile Fatty Acids

The accumulation of by-products, specifically volatile fatty acids (VFAs) and alcohols, was quantified at the end of each DF run using gas chromatography (GC). Liquid samples were centrifuged (5000 rpm, 5 min) and filtered through a 0.5 µm syringe filter. Analysis was performed using an Agilent 7890A gas chromatograph (Agilent Technologies LDA UK, Stockport, Cheshire, UK), equipped with a flame ionisation detector (FID) maintained at 200 °C. The system utilised a DB-FFAP column (30 m × 0.32 mm, film thickness of

0.5 µm) with nitrogen as make-up gas. A 10 µL sample volume was injected via an autosampler at a 5:1 split ratio, with the inlet port operated at 150 °C and helium as the carrier gas (10 mL/min). The column oven programme commenced at 60 °C (held for 4 min), increased to 140 °C at a ramp of 10 °C/min, and subsequently rose to 200 °C at 40 °C/min (held for 5 min). A commercial volatile acid standard mix (Merck Life Science UK Limited, Gillingham, Dorset, UK) and high-purity individual alcohol reagents were used for calibration. Data acquisition was performed using GC ChemStation software Rev. B.04.03-SP1 (Agilent Technologies LDA UK Limited, Stockport, Cheshire, UK).

2.8. Statistical Analysis

Biohydrogen yield data were analysed at a 95% confidence level ($p < 0.05$). The normality of the data distribution was assessed using the Shapiro–Wilk test ($p > 0.005$). All datasets conformed to normal distribution ($p > 0.05$), except for three outliers identified in the WH-BAB samples at 6, 12, and 18 h ($p < 0.05$). To determine the robustness of the results, statistical comparisons were conducted both with and without these outliers; as both approaches yielded identical outcomes, the use of non-parametric tests was deemed unnecessary. Hourly biohydrogen production in BABs was compared against the control CAB using a Student's *t*-test. Comparisons across various BAB configurations were performed via two-way ANOVA, with feedstock type (oakwood, OW; water hyacinth, WH) and pyrolysis temperature (450, 600, 650 °C) serving as independent variables. All statistical analyses and Gompertz nonlinear regression were carried out using SPSS Statistics 26 software.

3. Results

3.1. Biohydrogen Production and Kinetic Performance

Cumulative biohydrogen production during the dark fermentation with immobilised biochar–alginate beads (BAB) and control alginate beads (CAB) is exhibited in Figure 1. In the first batch (Figure 1a), biohydrogen generation commenced within the first hour for all BAB systems, whereas CAB exhibited a prolonged lag phase of ~15 h. BAB systems also reached a steady state significantly earlier (45–70 h) compared with CAB (88 h). The OW450, OW650, and WH450 systems outperformed the CAB yield by 9.42%, 12.04%, and 4.26%, respectively, with all differences being statistically significant ($p < 0.05$). While OW450 and OW650 achieved the highest final hydrogen yields, WH600 exhibited a more rapid onset of fermentation, albeit with a lower yield. Two-way ANOVA confirmed that both feedstock and pyrolysis temperature significantly influenced biohydrogen production ($p < 0.05$), highlighting the importance of biochar properties in modulating fermentative performance.

At the conclusion of the first batch, BABs remained physically stable, showing no visible swelling or structural failure, whereas CAB displayed slight swelling. No leakage of microbial inoculum or biochar from the beads into the reactor media was observed. HPLC analysis confirmed complete glucose consumption in all systems. Following substrate replenishment, a second consecutive batch was initiated using an acclimated consortium (Figure 1b). The BAB systems consistently outperformed CAB; high-temperature biochars facilitated higher experimental H_2 yields and more rapid fermentation kinetics. WH600 initiated biohydrogen production within 2 h and reached steady state by 128 h, whereas OW650 required 10 h to initiate and 149 h to stabilise. WH450 produced negligible biohydrogen during the first 88 h (0.25 mL H_2/g VS·h) but subsequently accelerated, reaching stability at 218 h. CAB performed the slowest, with negligible production (<0.025 mL H_2/g VS·h) during the first 96 h, only stabilising at 267 h (when biohydrogen changes were below 0.5%). Final biohydrogen yields for OW650, WH450, and WH600 were 269, 265, and 274 mL H_2/g VS, representing improvements of 20.8%, 19.1%, and 23.3% over CAB, respectively.

Kinetic parameters derived from the modified Gompertz model (Table 4) further elucidated these performance differences. In the first batch, CAB achieved the highest H_{max} (262 mL H_2/g VS) but with the lowest production rate (R_{max} = 3.3 mL H_2/g VS·h) and the longest lag phase (λ = 22 h). By contrast, WH600 exhibited the fastest kinetics (R_{max} = 8.7 mL H_2/g VS·h, λ = 12.6 h), reaching steady state much earlier despite a lower overall yield. Across all BAB systems, R_{max} was 1.4–2.6 times higher than CAB ($p < 0.05$), reflecting the beneficial role of biochar in accelerating biohydrogen generation. Although the reduction in λ for BAB relative to CAB was not statistically significant, the trend consistently favoured faster system initiation. Notably, WH600, despite producing less biohydrogen overall, reached steady state much earlier owing to its higher R_{max} and reduced λ.

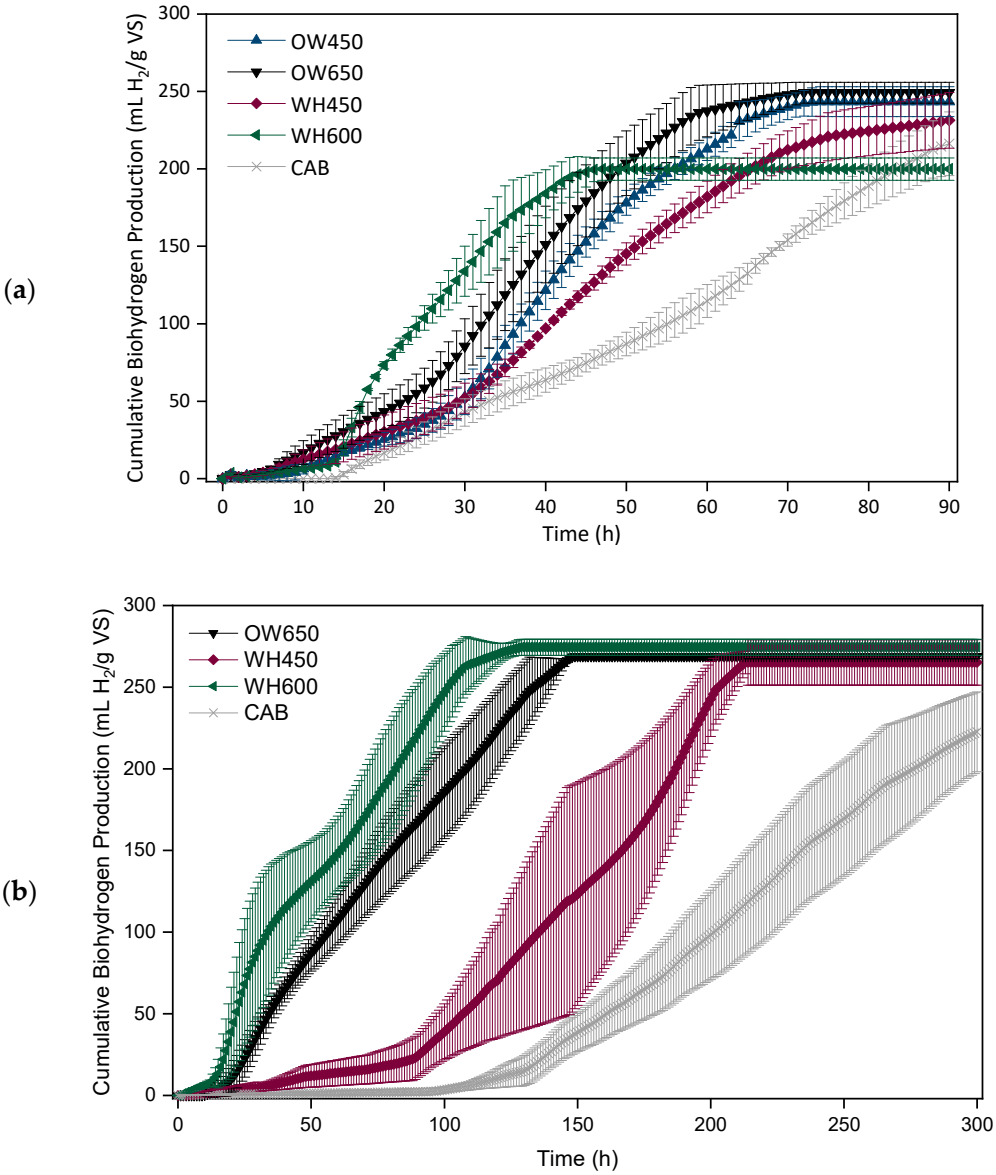

Figure 1. Biohydrogen production during dark fermentation of glucose with immobilised systems. (**a**) first batch; (**b**) second consecutive batch.

Kinetic parameters from the second batch confirmed this shift. WH450 achieved the highest H_{max} (290 mL H_2/g VS), while WH600 again delivered the most favourable kinetics (R_{max} = 3.2 mL H_2/g VS·h, λ = 8.5 h). Compared with CAB, OW650, WH450, and WH600 enhanced R_{max} by 73%, 47%, and 113% (1.5–2.1 times), while simultaneously reducing λ

by 85%, 32% and 94%, respectively. Although ANOVA revealed no statistically significant differences among biochar types for kinetic parameters, the consistent reduction in lag phase and acceleration of R_{max} across BAB systems demonstrated a clear kinetic advantage conferred by biochar immobilisation.

Mechanistically, these improvements are linked to the physicochemical characteristics of biochar. High-temperature pyrolysis (≥600 °C) enhances aromaticity, fixed carbon, surface area, and electrical conductivity, while concentrating ash and base cations to produce a more alkaline surface [22,33]. As shown in Table 1, OW650 (237 m^2/g) and WH600 (99 m^2/g) exhibited higher porosity, conductivity, aromaticity, and an enriched mineral composition compared to their low-temperature counterparts, OW450 (221 m^2/g) and WH450 (39 m^2/g). These features could promote efficient mass transfer and microbial immobilisation. The superior performance of OW650 and WH600 likely arises from a combination of increased porosity, enhanced electron transfer capacity, and the creation of favourable microenvironments for microbial activity.

Table 4. Experimental values and kinetic parameters calculated with the modified Gompertz model during microbial immobilisation in hybrid biochar–alginate beads for dark fermentation.

System	Initial pH	Final pH	H_{exp} (mL H_2/g VS)	H_{max} (mL H_2/g VS)	R_{max} (mL H_2/g VS·h)	λ (h)	R^2
First batch of dark fermentation							
OW450	6.2 ± 0.13	4.5 ± 0.03	243.4 ± 4.8	257.9 ± 15.2	6.4 ± 0.94	20.7 ± 7.8	0.997
OW650	6.0 ± 0.04	4.9 ± 0.07	249.3 ± 15.0	251.3 ± 16.7	6.7 ± 1.4	15.8 ± 1.0	0.981
WH450	5.8 ± 0.08	4.6 ± 0.06	232.0 ± 33.6	258.9 ± 25.5	4.5 ± 1.7	17.5 ± 4.0	0.997
WH600	6.0 ± 0.09	5.0 ± 0.12	199.8 ± 7.2	201.2 ± 8.9	8.7 ± 2.4	12.6 ± 1.4	0.997
CAB	6.2 ± 0.08	5.5 ± 0.12	222.5 ± 20.6	261.7 ± 38.3	3.3 ± 0.06	22.0 ± 1.5	0.992
Second consecutive batch of dark fermentation							
OW650	4.9 ± 0.12	4.9 ± 0.09	269.0 ± 1.5	285.5 ± 10.4	2.6 ± 0.2	19.2 ± 9.6	0.994
WH450	5.8 ± 0.25	5.8 ± 0.25	265.1 ± 7.0	290.3 ± 75.8	2.2 ± 0.8	89.8 ± 16.6	0.988
WH600	5.2 ± 0.09	4.0 ± 0.01	274.4 ± 4.9	282.7 ± 4.0	3.2 ± 0.5	8.5 ± 2.3	0.987
CAB	4.5 ± 0.07	3.8 ± 0.07	222.6 ± 24.5	298.3 ± 63.2	1.5 ± 0.4	131.7 ± 19.7	0.999

H_{exp}—experimental final biohydrogen yield, H_{max}—maximum biohydrogen potential, R_{max}—maximum specific biohydrogen production rate; λ is the lag phase duration.

The ash content of the oakwood biochars (OWBC450 11.7% and OWBC650 14.3%) was significantly lower than that of the water hyacinth biochars (WH 450 33.6% and WH600 42.6%), suggesting that both the amount and distribution of mineral ash are primarily determined by the feedstock. The chemical composition of WH is highly dependent on its growing environment, owing to the inherent capacity of the plant for the uptake of inorganic compounds and heavy metals from aquatic systems [34]. As the pyrolysis temperature increases, inorganic constituents within the biochar concentrate due to the loss of C, H and O through volatilisation. XRF analysis of biochars (Table 2) indicated a predominance of Fe, K, Ca, Mg, Al and Si. These minerals likely complement microbial nutrient requirements, thereby enhancing fermentative performance. Specifically, biochar could supply Fe, Ca and K—essential elements for microbial growth and the enzymatic activity required for the acetic and butyric acid fermentation pathways. Interestingly, the most favourable performance was observed with the high-temperature biochars, which also possessed the highest inorganic content. Previous reports on DF with suspended cells support these findings, demonstrating significant increases in H_2 yields when employing biochar compared to suspended controls. For instance, rice straw biochar (produced at 700 °C) increased H_2 yields by 27–118% [35], while pine wood biochar (650 and 900 °C) enhanced H_2 yields by 89% and 128%, respectively [36]. These studies attributed such improvements

to the mineral-rich nature of the biochar, which facilitates higher H_2 yields and production rates, encourages the proliferation of *Clostridium spp.*, and promotes the production of acetic acid and butyric acid. Furthermore, biochar functions as an effective immobilisation support, facilitating synergistic interactions among microbial species. While the alginate matrix alone provides spatial proximity between cells, the additional physicochemical benefits provided by the biochar—specifically its mineral content and electrochemical properties—likely account for the superior improvements observed in this study.

3.2. pH Dynamics and Volatile Fatty Acids

At the onset of the first batch, the BAB systems naturally stabilised near pH 6—a range suitable for fermentative biohydrogen producers (optimal pH 5–7) [4]—whereas CAB and the blank control required manual acid adjustment (Table 4). After 90 h, fermentation ceased as pH levels declined to 4.5–5.5. Systems containing intermediate-temperature biochars showed greater acidification, with OW650 (pH 4.9) and WH600 (pH 5.0) maintaining lower terminal pH values than CAB (pH 5.5). In the second batch, initial pH ranged from 4.5 to 5.8 and decreased further; CAB eventually reached 3.8, falling below the operational threshold for H_2 generation, where severe inhibition occurs [37]. The relatively higher final pH in BABs could be attributed to the inherent buffering and redox-active properties of the biochar. pH levels critically shape DF by regulating hydrogenase activity and directing metabolic pathways. Generally, acidic conditions favour H_2-producing bacteria (e.g., *Clostridium* spp.), whereas neutral or alkaline conditions tend to promote the proliferation of H_2-oxidising methanogens [18]. Immobilisation within biochar–alginate beads likely enhances cell-support interactions through surface charge modifications [38]. XPS analysis indicates that increasing pyrolysis temperature decreases the concentration of oxygenated groups (C–O, COO) while simultaneously enriching basic N functionalities. This results in the formation of more hydrophobic, alkaline surfaces that are significantly more conducive to microbial adhesion [28].

VFA profiles corroborated these trends. In the first batch, BABs predominantly followed the acetic acid pathway (319–364 mg/L), with lower ethanol (130–383 mg/L) and butyrate (60–118 mg/L) concentrations (Figure 2a). In contrast, CAB exhibited minimal VFA accumulation, consistent with its lower biohydrogen yield. The dominance of the acetic acid metabolic pathway (Equation (3)) is significant, as it provides the highest H_2 recovery from glucose, followed by the butyric acid pathway (Equation (4)). Conversely, the propionate pathway consumes H_2, thereby reducing the overall yield. Similarly, the ethanol and butanol pathways divert intracellular reducing equivalents (NADH) away from hydrogenases, limiting their availability for H_2 production [14,39].

$$\textbf{Acetate pathway: } C_6H_{12}O_6 + 2H_2O \rightarrow 2\,CH_3COOH + 2CO_2 + 4H_2 \quad (3)$$

$$\textbf{Butyrate pathway: } C_6H_{12}O_6 \rightarrow CH_3CH_2CH_2COOH + 2CO_2 + 2H_2 \quad (4)$$

The second batch exhibited greater VFA accumulation, most notably in CAB, which produced nearly tenfold more than in the first run (Figure 2b). BABs showed more moderate increases; OW650 and WH600 boosted VFA levels by 78% and 15%, respectively, while WH450 decreased by 57%. Acetic acid remained the dominant VFA (54–80% of total VFAs), followed by ethanol (4–35%) and butyrate (5–10%). The prevalence of acetate in BAB systems likely underpinned their enhanced H_2 yields across both batches. These results suggest that biochar-mediated immobilisation modulates both pH buffering and metabolic routing, steering the microbial consortium toward acetate-driven pathways and away from less favourable ethanol or propionate routes. Such changes are outlined in Figure 3 by comparing the average shift in VFA composition between the first and second batch of

DF, illustrating the increased predominance of acetic acid. This behaviour is consistent with previous reports that biochar enriches hydrogenic bacteria, particularly spore-forming *Clostridium*, while suppressing less efficient fermenters [2,40].

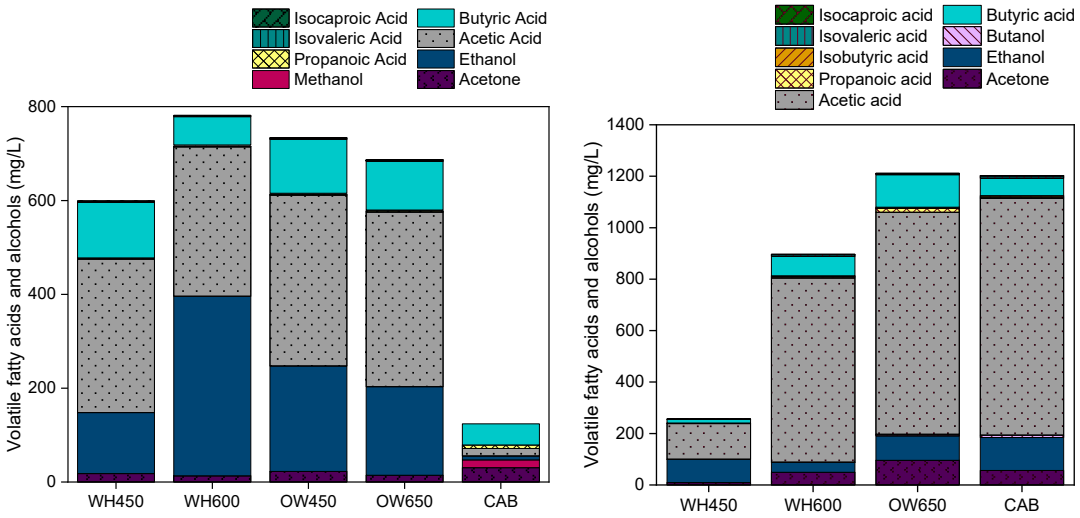

Figure 2. Volatile fatty acids and alcohols accumulated at the end of the dark fermentation of the immobilised systems: (**a**) first DF batch; (**b**) second DF batch.

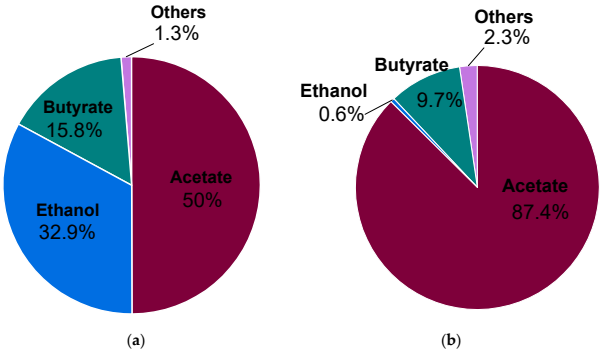

Figure 3. Shift in metabolic pathways of dark fermentation determined by the average volatile fatty acids composition: (**a**) first batch VFA profile; (**b**) second batch VFA profile.

3.3. Potential of Biochar–Alginate Beads as an Immobilisation Support

The present study demonstrates that biochar–alginate hybrid beads constitute an effective immobilisation matrix for enhancing biohydrogen production during DF. Although biochar supplementation has been widely investigated in anaerobic digestion for methane generation [41], its application as structured immobilisation support in DF remains largely unexplored, leaving a distinct lack of clear guidelines regarding which biochar types confer the greatest operational benefits. In a related study, Ngamnurak et al. [42] employed BAB systems for the DF of food waste, evaluating the performance of cassava rhizome BC pyrolysed at 400 °C across a BC dosage range of 0–3% (*w*/*v*) and bead diameters of 1–7 mm. The reported H_2 production for the BAB systems ostensibly outperformed both CAB and the suspended control (Table 5). The optimum performance was achieved at a 2% BC loading and a 2 mm bead diameter, albeit resulting in a considerably low yield of 17.24 mL H_2/g VS. The authors asserted that the BAB matrix shielded the microorganisms from VFA accumulation and established a favourable microenvironment, while the porosity of the BC enhanced mass transfer, provided localised buffering capacity, and supported biofilm

formation. However, the surface area of this BC was remarkably low (1.66 m^2/g), thereby limiting the efficacy of these structural attributes. Notably, their discussion was primarily limited to average values, with H_2 yields and production rates presented exclusively in graphical form using non-standardised units (mmol H_2/g COD), except for isolated yield data expressed in the conventional mL H_2/g VS units.

The broader deployment of biochar in gaseous biofuel production is currently constrained by challenges regarding availability, production costs, dosing, and, critically, the lack of standardisation due to its heterogeneous composition, which varies significantly with feedstock and pyrolysis conditions [16]. Among the physicochemical determinants of biochar performance, pyrolysis temperature and feedstock composition are paramount. Increasing pyrolysis temperature promotes the release of O- and H-containing functional groups as aliphatic structures condense into more thermodynamically stable aromatic domains [43]. This transition results in biochars with reduced surface functionality but higher conductivity, aromaticity, and structural stability. In contrast, intermediate-temperature biochars typically retain greater surface functionality and cation exchange capacity (CEC). Both surface area and surface chemistry are critical for immobilisation: a large surface area provides abundant adsorption sites and facilitates mass transfer, while appropriate surface functional groups can promote electrostatic interactions and microbial attachment [21,22].

This work demonstrates that higher-temperature biochars reduce the lag phase, accelerate biohydrogen production rates, and shift metabolism towards the acetate pathway—consistent with more efficient hydrogenic routes. These findings align with previous reports (Table 5). Bu et al. [40] showed that biochar derived from dried leaves (produced at 600 °C) outperformed lower-temperature analogues in DF of pretreated sugarcane bagasse, tripling H_2 yields relative to the control while favouring acetate and ethanol accumulation. The improvement was linked to enhanced electrochemical activity, greater biofilm formation, and increased hydrogenase and cellulase activities, along with a higher intracellular $NADH/NAD^+$ ratio, which bolstered electron availability. Similarly, Huang et al. [44] reported that high-temperature leaf biochar (600 °C) improved H_2 production for *Thermoanaerobacterium thermosaccharolyticum* MJ2 by sustaining pH stability, stimulating bacterial growth, and reinforcing acetate/ethanol pathways. Yang and Wang [44] found that sawdust biochar produced at intermediate temperature (500 °C) enhanced H_2 and VFA production by promoting biofilm formation, shielding microbes from inhibitors, providing nutrients, and stimulating dehydrogenase activity—effects that were further amplified when combined with Fe nanoparticles. Minerals naturally present in biochar, such as Fe, Ca, and K, have also been suggested to complement microbial nutrient requirements and improve fermentative performance [45].

Discrepancies in reporting—specifically the use of various units (mL H_2/g VS, mL H_2/L, mol H_2/mol substrate, mol H_2/g COD, mL H_2/L·h)—complicate direct comparisons and highlight the necessity for standardising data representation. Many studies report pyrolysis temperature and feedstock but fail to include a standardised characterisation of the biochar (e.g., surface area, composition and surface functionality) that could link these properties to performance. Taken together, these results underscore the potential of biochar–alginate beads as multifunctional immobilisation supports. Beyond providing structural stability, biochar contributes electrochemical conductivity, buffering capacity, and nutrient supplementation, thereby fostering robust and metabolically favourable hydrogenic consortia. Table 5 demonstrates that carbonaceous supports can substantially increase biohydrogen production, although other factors, such as biochar dosage, substrate selection, and reactor operation, require further attention. Future optimisation should focus on standardising biochar properties and tuning feedstock–pyrolysis combinations to maximise performance in DF systems.

Table 5. Reports of carbonaceous material addition during mesophilic dark fermentation.

Inoculum and Pre-Treatment	Biochar/Activated Carbon	Operating Conditions	H_2 Yield	H_2 Rate	Reference
Anaerobic sludge autoclaved at 115 °C for 30 min	Oak wood BC 450/650 °C; water hyacinth BC 450/600 °C, 1 h	AMPTS, hybrid biochar–alginate beads; control alginate beads (CAB), glucose 5 g VS/L, initial pH 6	OW450: 243 mL H_2/g VS OW650: 249 mL H_2/g VS WH450: 232 mL H_2/g VS WH600: 200 mL H_2/g VS CAB: 223 mL H_2/g VS	OW450: 6.4 mL H_2/g VS·h OW650: 6.7 mL H_2/g VS·h WH450: 4.5 mL H_2/g VS·h WH600: 8.7 mL H_2/g VS·h CAB: 3.3 mL H_2/g VS·h	This work
Petroleum waste sludge heated at 105 °C for 2 h	Cassava rhizome BC 400 °C for 1 day	60 mL bottles, 6 g biochar–alginate beads, food waste 20 g COD/L, pH 6	BAB: 340–690 mol H_2/gCOD CAB: 330 mol H_2/g COD SC: 8 mol H_2/g COD	BAB: 7–20 mol H_2/g COD·h CAB: 0.4 mol H_2/g COD·h SC: 0.6 mol H_2/g COD·h	[42]
Thermoanaerobacterium thermosaccharolyticum MJ2	Fallen leaves BC 600 °C for 1 h.	55 mL bottles, 10% inoculum, PSBC 10 g/L, BC 7 g/L	BC: 395mL H_2/g VS SC: 192 mL H_2/g VS	NR	[5]
Anaerobic sludge heated at 90 °C for 15 min	Fallen leaves BC 300, 450, and 600 °C for 2 h.	120 mL bottles, WV 50 mL, 10% (v/v) inoculum, 10 g/L PSCB, BC 10 g/L	BC 300: 721 mL H_2/L BC 450: 1069 mL H_2/L BC 600: 2724 mL H_2/L SC: 690 mL H_2/L	BC 300: 13.4 mL H_2/L·h BC 450: 40.3 mL H_2/L·h BC 600: 121 mL H_2/L·h SC: 17.9 mL H_2/L·h	[40]
Anaerobic sludge heated at 95 °C for 30 min	Pinewood BC pretreated with citric acid 650, 900 °C, 20 min	100 mL serum bottles, WV 60 mL, bread 8 g VS/L, initial pH 6.4, BC 15 g/L	BC 650: 957 mL H_2/L BC 900: 1154 mL H_2/L SC: 507 mL H_2/L	BC 650: 26.1 mL H_2/L·h BC 900: 28.7 mL H_2/L·h	[36]
Clostridium tyrobutyricum for butyrate and *Ethanoligenens harbinense* for ethanol fermentation	Rice straw BC 700 °C for 4 h	160 mL serum bottle, WV 50 mL, glucose 15 g/L, 37 °C, initial pH adjusted to 7 before adding biochar. Biochar dosage of 0, 3, 6, 9 and 12 g/L	Ethanol fermentation BC 3 g/L: 125.87 mL H_2 BC 6 g/L: 125.9 mL H_2 BC 9 g/L: 122.7 mL H_2 BC 12 g/L:117.5 mL H_2 SC: 57.64 mL H_2 Butyrate fermentation BC 3 g/L: 190.5 mL H_2 BC 6 g/L: 197.2 mL H_2 BC 9 g/L: 191.6 mL H_2 BC 12 g/L: 182.8 mL H_2 SC: 106.1 mL H_2	Ethanol fermentation BC 3 g/L: 6.2 mL H_2/h BC 6 g/L: 6.0 mL H_2/h BC 9 g/L: 5.7 mL H_2/h BC 12 g/L: 6.0 mL H_2/h SC: 1.9 mL H_2/h Butyrate fermentation BC 3 g/L: 5.0 mL H_2/h BC 6 g/L: 6.9 mL H_2/h BC 9 g/L: 11.4 mL H_2/h BC 12 g/L: 11.4 mL H_2/h SC: 2.7 mL H_2/h	[35]

Table 5. *Cont.*

Inoculum and Pre-Treatment	Biochar/Activated Carbon	Operating Conditions	H_2 Yield	H_2 Rate	Reference
Anaerobic sludge heated at 100 °C for 15 min	Sawdust BC 500 °C for 2 h	150 mL bottle, WV 100 mL, grass 1 g VS, inoculum 30 mL, BC 0.6 g/L, Fe-NP 0.4 g/L	BC:30.9 mL H_2/g Fe-NP: 40.9 mL H_2/g BC-Fe-NP: 50.6 mL H_2/g SC: 26.6 mL H_2/g	NR	[44]
Anaerobic sludge heated 80 °C for 1 h	Activated carbon	Batch 150 mL bottle, 60 mL WV; 1 L CSTR HRT 16 h; JWH; beads Na-alginate 2%, AC 1%, chitosan 1% and SiO_2 1%	Batch: 3 mL H_2/g CSTR: 7 mL H_2/g	Batch: 1.25 mL H_2/L·h CSTR: 32.7 mL H_2/L·h	[46]
Anaerobic sludge pH 10 for 1 d, then pH 7, and boiled for 30 min	Carbon nanotubes (CNTs) and activated carbon	UASB, WV 5L, support 100 mg/L, glucose 10 g/L, pH 6.5, inoculum 20% (*v*/*v*); HRT 24 h; after 2 weeks OLR 20 g/L·d	CNTs: 2.45 mol H_2/mol AC: 1.42 mol H_2/mol SC: washout after 2 weeks	CNTs: 0.78 L H_2/L·h AC: 0.48 L H_2/L·h	[10]

AC—activated carbon; AMPTS—automatic methane potential test system; BC—biochar; CMISR—continuous mixed immobilised sludge reactor; CSTR—continuous stirred tank reactor; Fe-NP—iron nanoparticles; HRT—hydraulic retention time; IPR—inoculum to packing ratio; JWH—jatropha waste hydrolysate; NR—not reported; OLR—organic loading rate; PSCB—pretreated sugarcane bagasse; SC—suspended control; UASB—up-flow anaerobic sludge blanket; WV—working volume.

4. Conclusions

The incorporation of biochar into alginate beads for hybrid cell immobilisation markedly enhanced experimental biohydrogen production during dark fermentation by shortening the lag phase. Biohydrogen yields for BAB systems were 4.26–12.04% and 19.1–20.8% higher than those of CAB during the first and second batches, respectively. The production rate was the kinetic parameter that showed the most significant improvement, being 1.4–2.6 times higher with BAB than with CAB in both runs. High-temperature biochars proved most effective, suggesting that severe carbonisation confers physicochemical properties favourable to microbial activity. Increased porosity and surface likely facilitated mass transfer and active cell loading, while enhanced electrical conductivity may have promoted synergistic microbial interactions. Moreover, the redox and buffering capacities of the biochars supported acetic acid as the predominant by-product, thereby steering metabolism towards the most efficient hydrogen-generating pathway. The combined adsorption-entrapment architecture couples the advantages of the biochar with the protective, high-biomass environment of alginate beads, resulting in higher biohydrogen yields and rates. The successful performance of a second consecutive batch underscores the importance of microbial acclimatisation and highlights the potential of hybrid biochar–alginate immobilised systems for extended or continuous operation. These outcomes align with the consensus that the immobilisation of mixed consortia can significantly increase biohydrogen productivity and process stability. Nevertheless, future investigations would benefit from incorporating scanning electron microscopy (SEM) to visualise the matrix structure and biofilm formation, alongside microbial DNA sequencing (16S rRNA) to evaluate community proliferation.

Author Contributions: Conceptualization, J.Q.-N. and A.B.R.; methodology, J.Q.-N. and J.E.B.-G.; software, J.Q.-N.; validation, J.Q.-N. and A.B.R.; formal analysis, J.Q.-N.; investigation, J.Q.-N.; resources, J.Q.-N. and A.B.R.; data curation, J.Q.-N.; writing—original draft preparation, J.Q.-N. and J.E.B.-G.; writing—review and editing, J.Q.-N., J.E.B.-G. and A.B.R.; visualisation, J.Q.-N., J.E.B.-G. and A.B.R.; supervision, A.B.R.; project administration, A.B.R.; funding acquisition, J.Q.-N. and A.B.R. All authors have read and agreed to the published version of the manuscript.

Funding: This research was funded by the National Council on Science and Technology and the Mexican Secretariat of Energy (CONACYT-SENER), and the Biotechnology and Biological Sciences Research Council (BBSRC) and Global Challenges Research Fund (GCRF) through the project BEFWAM Bioenergy, Fertilisers, and clean Water from invasive Aquatic Macrophytes [grant BB/S011439/1].

Data Availability Statement: Dataset available on request from the authors.

Acknowledgments: The authors gratefully acknowledge the partners from the collaborative BEFWAM project that collected and provided the water hyacinth samples; Department of Chemical Engineering, Institute of Chemical Technology, Mumbai, India; Visva-Bharati University; Centre for Research in Energy and Energy Conservation (CREEC) at Makerere University, Uganda; Defiant Renewables, India; Green Heat, Uganda. The authors are also thankful to Callym Munro for his help with the experimental setup and the Esholt Wastewater Treatment Plant for providing inoculum samples.

Conflicts of Interest: The authors declare no conflicts of interest.

Abbreviations

The following abbreviations are used in this manuscript:

AC	Activated carbon
AMPTS	Automatic methane potential test system
BAB	biochar–alginate beads

BC	Biochar
BET	Brunauer, Emmett, and Teller
CAB	Control alginate beads
CEC	Cation exchange capacity
CMISR	Continuous mixed immobilised sludge reactor
CNTs	Carbon nanotubes
CSTR	Continuous stirred tank reactor
DIET	Direct interspecies electron transfer
DF	Dark fermentation
GHG	Greenhouse gases
HRT	Hydraulic retention time
IPR	Inoculum to packing ratio
NADH	Nicotinamide adenine dinucleotide
NR	Not reported
OFG	Oxygenated functional group
OLR	Organic loading rate
OW	Oakwood
PSCB	Pretreated sugarcane bagasse
SA	Surface area
SC	Suspended control
SEM	Scanning Electron Microscopy
UASB	Up-flow anaerobic sludge blanket
VFA	Volatile fatty acids
VS	Volatile solids
WH	Water hyacinth
WV	Working volume
μ_m	Biohydrogen production rate
λ	Lag phase

References

1. IEA The Future of Hydrogen. Available online: https://www.iea.org/ (accessed on 7 May 2020).
2. Arun, J.; Sasipraba, T.; Gopinath, K.P.; Priyadharsini, P.; Nachiappan, S.; Nirmala, N.; Dawn, S.S.; Chi, N.T.L.; Pugazhendhi, A. Influence of Biomass and Nanoadditives in Dark Fermentation for Enriched Bio-Hydrogen Production: A Detailed Mechanistic Review on Pathway and Commercialization Challenges. *Fuel* **2022**, *327*, 125112. [CrossRef]
3. Mudhoo, A.; Forster-Carneiro, T.; Sánchez, A. Biohydrogen Production and Bioprocess Enhancement: A Review. *Crit. Rev. Biotechnol.* **2011**, *31*, 250–263. [CrossRef] [PubMed]
4. Łukajtis, R.; Hołowacz, I.; Kucharska, K.; Glinka, M.; Rybarczyk, P.; Przyjazny, A.; Kamiński, M. Hydrogen Production from Biomass Using Dark Fermentation. *Renew. Sustain. Energy Rev.* **2018**, *91*, 665–694. [CrossRef]
5. Huang, J.-R.; Chen, X.; Hu, B.-B.; Cheng, J.-R.; Zhu, M.-J. Bioaugmentation Combined with Biochar to Enhance Thermophilic Hydrogen Production from Sugarcane Bagasse. *Bioresour. Technol.* **2022**, *348*, 126790. [CrossRef] [PubMed]
6. Kannah, R.Y.; Kavitha, S.; Karthikeyan, O.P.; Kumar, G.; Dai-Viet, N.V.; Banu, J.R. Techno-Economic Assessment of Various Hydrogen Production Methods—A Review. *Bioresour. Technol.* **2021**, *319*, 124175. [CrossRef] [PubMed]
7. Jayachandran, V.; Basak, N.; De Philippis, R.; Adessi, A. Novel Strategies towards Efficient Molecular Biohydrogen Production by Dark Fermentative Mechanism: Present Progress and Future Perspective. *Bioprocess Biosyst. Eng.* **2022**, *45*, 1595–1624. [CrossRef] [PubMed]
8. Mudhoo, A.; Torres-Mayanga, P.C.; Forster-Carneiro, T.; Sivagurunathan, P.; Kumar, G.; Komilis, D.; Sánchez, A. A Review of Research Trends in the Enhancement of Biomass-to-Hydrogen Conversion. *Waste Manag.* **2018**, *79*, 580–594. [CrossRef] [PubMed]
9. Park, J.; Sim, Y.; Kim, J.S.; Kim, S. Effects of Alginate Immobilization on Dynamic Membrane Formation and H2 Fermentation from Galactose. *Int. J. Hydrogen Energy* **2020**, *45*, 5874–5880. [CrossRef]
10. Liu, Z.; Lv, F.; Zheng, H.; Zhang, C.; Wei, F.; Xing, X.-H. Enhanced Hydrogen Production in a UASB Reactor by Retaining Microbial Consortium onto Carbon Nanotubes (CNTs). *Int. J. Hydrogen Energy* **2012**, *37*, 10619–10626. [CrossRef]
11. Seelert, T.; Ghosh, D.; Yargeau, V. Improving Biohydrogen Production Using Clostridium Beijerinckii Immobilized with Magnetite Nanoparticles. *Appl. Microbiol. Biotechnol.* **2015**, *99*, 4107–4116. [CrossRef] [PubMed]

12. Gokfiliz, P.; Karapinar, I. The Effect of Support Particle Type on Thermophilic Hydrogen Production by Immobilized Batch Dark Fermentation. *Int. J. Hydrogen Energy* **2017**, *42*, 2553–2561. [CrossRef]
13. Muri, P.; Marinšek-Logar, R.; Djinović, P.; Pintar, A. Influence of Support Materials on Continuous Hydrogen Production in Anaerobic Packed-Bed Reactor with Immobilized Hydrogen Producing Bacteria at Acidic Conditions. *Enzym. Microb. Technol.* **2018**, *111*, 87–96. [CrossRef] [PubMed]
14. Kumar, G.; Buitrón, G. Fermentative Biohydrogen Production in Fixed Bed Reactors Using Ceramic and Polyethylene Carriers as Supporting Material. *Energy Procedia* **2017**, *142*, 743–748. [CrossRef]
15. Nunes Ferraz Júnior, A.D.; Etchebehere, C.; Zaiat, M. Mesophilic Hydrogen Production in Acidogenic Packed-Bed Reactors (APBR) Using Raw Sugarcane Vinasse as Substrate: Influence of Support Materials. *Anaerobe* **2015**, *34*, 94–105. [CrossRef] [PubMed]
16. Sirohi, R.; Vivekanand, V.; Pandey, A.K.; Tarafdar, A.; Awasthi, M.K.; Shakya, A.; Kim, S.H.; Sim, S.J.; Tuan, H.A.; Pandey, A. Emerging Trends in Role and Significance of Biochar in Gaseous Biofuels Production. *Environ. Technol. Innov.* **2023**, *30*, 103100. [CrossRef]
17. Sánchez, P.; Hernández, R.M.; Pedraz, J.L.; Orive, G. Encapsulation of Cells in Alginate Gels. In *Immobilization of Enzymes and Cells*; Guisan, J.M., Ed.; Humana Press: Totowa, NJ, USA, 2013; Volume 1051, pp. 313–325.
18. Kumar, G.; Mudhoo, A.; Sivagurunathan, P.; Nagarajan, D.; Ghimire, A.; Lay, C.-H.; Lin, C.-Y.; Lee, D.-J.; Chang, J.-S. Recent Insights into the Cell Immobilization Technology Applied for Dark Fermentative Hydrogen Production. *Bioresour. Technol.* **2016**, *219*, 725–737. [CrossRef] [PubMed]
19. Bu, J.; Ju, X.; Liang, L.; Zhao, Q.; Wei, Y.; Wu, H. Molecular Mechanism of Boosted Hydrogen Production by Thermoanaerobacterium Thermosaccharolyticum with Biochar Revealed by Transcriptome Analysis. *Chem. Eng. J.* **2024**, *500*, 156903. [CrossRef]
20. Kozłowski, K.; Dach, J.; Czekała, W.; Malińska, K.; Świechowski, K.; Pulka, J.; Lewicki, A. Influence of the Parameters of Used Biochar on the Dark Fermentation Process. *Energies* **2023**, *16*, 7484. [CrossRef]
21. Leng, L.; Xiong, Q.; Yang, L.; Li, H.; Zhou, Y.; Zhang, W.; Jiang, S.; Li, H.; Huang, H. An Overview on Engineering the Surface Area and Porosity of Biochar. *Sci. Total Environ.* **2021**, *763*, 144204. [CrossRef] [PubMed]
22. Weber, K.; Quicker, P. Properties of Biochar. *Fuel* **2018**, *217*, 240–261. [CrossRef]
23. Klüpfel, L.; Keiluweit, M.; Kleber, M.; Sander, M. Redox Properties of Plant Biomass-Derived Black Carbon (Biochar). *Environ. Sci. Technol.* **2014**, *48*, 5601–5611. [CrossRef] [PubMed]
24. Bray, D.G.; Nahar, G.; Grasham, O.; Dalvi, V.; Rajput, S.; Dupont, V.; Camargo-Valero, M.A.; Ross, A.B. The Cultivation of Water Hyacinth in India as a Feedstock for Anaerobic Digestion: Development of a Predictive Model for Scaling Integrated Systems. *Energies* **2022**, *15*, 9599. [CrossRef]
25. Irewale, A.T.; Dimkpa, C.O.; Elemike, E.E.; Oguzie, E.E. Water Hyacinth: Prospects for Biochar-Based, Nano-Enabled Biofertilizer Development. *Heliyon* **2024**, *10*, e36966. [CrossRef] [PubMed]
26. Teli, A.; Ficara, E.; Malpei, F. Bio-Hydrogen Production from Cheese Whey by Dark Fermentation. *Chem. Eng. Trans.* **2014**, *37*, 613–618. [CrossRef]
27. *APHA Standard Methods for the Examination of Water and Wastewater*; APHA Press: Washington DC, USA, 2005.
28. Quintana-Najera, J.; Blacker, A.J.; Fletcher, L.A.; Ross, A.B. The Effect of Augmentation of Biochar and Hydrochar in Anaerobic Digestion of a Model Substrate. *Bioresour. Technol.* **2021**, *321*, 124494. [CrossRef] [PubMed]
29. Tarazona, P.; Marconi, U.M.B.; Evans, R. Phase Equilibria of Fluid Interfaces and Conflned Fluids Non-Local versus Local Density Functionals. *Mol. Phys.* **1987**, *60*, 573–595. [CrossRef]
30. Watts, J.F.; Wolstenholme, J. *An Introduction to Surface Analysis by XPS and AES*; John Wiley & Sons: Hoboken, NJ, USA, 2003.
31. Smidsrød, O.; Skjak-Braek, G. Alginate as Immobilization Matrix for Cells. *Trends Biotechnol.* **1990**, *8*, 71–78. [CrossRef] [PubMed]
32. Barrera-Quintero, V.; Davila-Gomez, J.A.; Acosta, P.R.; Hernandez-Rojas, M.E.; Baez-Pimiento, S. Gompertz Equation's First and Second Derivatives for Kinetics Analysis of Batch Dark Fermentation on Bio-Hydrogen Production. *Eur. J. Eng. Technol. Res.* **2017**, *2*, 18–22. [CrossRef]
33. Mafu, L.D.; Neomagus, H.W.J.P.; Everson, R.C.; Strydom, C.A.; Carrier, M.; Okolo, G.N.; Bunt, J.R. Chemical and Structural Characterization of Char Development during Lignocellulosic Biomass Pyrolysis. *Bioresour. Technol.* **2017**, *243*, 941–948. [CrossRef] [PubMed]
34. Jones, J.L.; Jenkins, R.O.; Haris, P.I. Extending the Geographic Reach of the Water Hyacinth Plant in Removal of Heavy Metals from a Temperate Northern Hemisphere River. *Sci. Rep.* **2018**, *8*, 11071. [CrossRef] [PubMed]
35. Li, W.; He, L.; Cheng, C.; Cao, G.; Ren, N. Effects of Biochar on Ethanol-Type and Butyrate-Type Fermentative Hydrogen Productions. *Bioresour. Technol.* **2020**, *306*, 123088. [CrossRef] [PubMed]
36. Sugiarto, Y.; Sunyoto, N.M.S.; Zhu, M.; Jones, I.; Zhang, D. Effect of Biochar in Enhancing Hydrogen Production by Mesophilic Anaerobic Digestion of Food Wastes: The Role of Minerals. *Int. J. Hydrogen Energy* **2021**, *46*, 3695–3703. [CrossRef]
37. Aghajani Delavar, M.; Wang, J. Numerical Investigation of PH Control on Dark Fermentation and Hydrogen Production in a Microbioreactor. *Fuel* **2021**, *292*, 120355. [CrossRef]

38. Quirós, M.; García, A.B.; Montes-Morán, M.A. Influence of the Support Surface Properties on the Protein Loading and Activity of Lipase/Mesoporous Carbon Biocatalysts. *Carbon* **2011**, *49*, 406–415. [CrossRef]
39. Cao, Y.; Liu, H.; Liu, W.; Guo, J.; Xian, M. Debottlenecking the Biological Hydrogen Production Pathway of Dark Fermentation: Insight into the Impact of Strain Improvement. *Microb. Cell Fact.* **2022**, *21*, 166. [CrossRef] [PubMed]
40. Bu, J.; Wei, H.-L.; Wang, Y.-T.; Cheng, J.-R.; Zhu, M.-J. Biochar Boosts Dark Fermentative H2 Production from Sugarcane Bagasse by Selective Enrichment/Colonization of Functional Bacteria and Enhancing Extracellular Electron Transfer. *Water Res.* **2021**, *202*, 117440. [CrossRef] [PubMed]
41. Quintana-Najera, J.; Blacker, A.J.; Fletcher, L.A.; Ross, A.B. Understanding the Influence of Biochar Augmentation in Anaerobic Digestion by Principal Component Analysis. *Energies* **2023**, *16*, 2523. [CrossRef]
42. Ngamnurak, P.; Plangklang, P.; Pomdaeng, P.; Ko, T.W.; Reungsang, A.; Chu, C.Y. Synergistic Sodium Alginate- and Biochar-Immobilized Cells for Enhancing Fermentative Hydrogen Production from Food Waste. *Environ. Sci. Pollut. Res.* **2024**, *31*, 64524–64533. [CrossRef] [PubMed]
43. Chan, K.Y.; Xu, Z. Biochar: Nutrient Properties and Their Enhancement. In *Biochar for Environmental Management: Science and Technology*; Routledge: London, UK, 2009; pp. 99–116.
44. Yang, G.; Wang, J. Synergistic Enhancement of Biohydrogen Production from Grass Fermentation Using Biochar Combined with Zero-Valent Iron Nanoparticles. *Fuel* **2019**, *251*, 420–427. [CrossRef]
45. Sugiarto, Y.; Sunyoto, N.M.S.; Zhu, M.; Jones, I.; Zhang, D. Effect of Biochar Addition on Microbial Community and Methane Production during Anaerobic Digestion of Food Wastes: The Role of Minerals in Biochar. *Bioresour. Technol.* **2021**, *323*, 124585. [CrossRef] [PubMed]
46. Kumar, G.; Sivagurunathan, P.; Sen, B.; Kim, S.; Lin, C. Mesophilic Continuous Fermentative Hydrogen Production from Acid Pretreated De-Oiled Jatropha Waste Hydrolysate Using Immobilized Microorganisms. *Bioresour. Technol.* **2017**, *240*, 137–143. [CrossRef] [PubMed]